Military Technical College
Kobry El-Kobbah,
Cairo, Egypt.

13th International Conference on Applied Mechanics and Mechanical Engineering.

ANAYSIS AND CONTROL LAWS OF SEMI-ACTIVE VEHICLE SUSPENSION SYSTEMS WITH RENDING AN ACCOUNT OF THE PHYSICAL CHARACTERISTICS OF MAGNETO-RHEOLOGICAL DAMPERS

GENOVE** J., TASHKOV* S., TRAYKOV**** B., ARNAUDOV*** K. and VENKOV*** G.

ABSTRACT

In the paper, comparative analysis of the semi-active suspension systems effectiveness towards the passive ones is studied. Several control laws are investigated depending on the analyses goals–comfort increasing, stability improvement or a realized compromise between them. There are suggested few implemented controller types, and their effectiveness is discussed. The influence upon the effectiveness of the damper nonlinear physical model is analyzed.

KEY WORDS

Semi-active Suspension, Automotive, MR Damper

ABBREVIATION

AFC – Amplitude Frequency Characteristics
ER – Electro-rheological
MR – Magneto-rheological
NN – Neural Network
PFC – Phase Frequency Characteristics
PWM – Pulse Width Modulator
TF – Transfer Function
Vabs – Absolute velocity

A, B, C, D – State Space Matrices
c – Elastic Constant

* Assistant professor, Dpt. of Mech. Power, Technical University, Sofia, Bulgaria.
** Associate professor, Dpt. of Mech., Technical University, Sofia, Bulgaria.
*** Professor, Dpt. Mech., Technical University, Sofia, Bulgaria.
**** Professor, Dpt. Transport Technologies, Technical University, Sofia, Bulgaria.

b – Damping Constant
z – Absolute Coordinate
ξ – Road Excitation

INTRODUCTION

The main goals of suspension synthesis of the vehicle are:

- to provide ride comfort, that is to protect the driver, the passengers and cargo against vibration impact due to irregularities of the road surface;
- to reduce dynamic wheel forces, to gain enough dynamic steering stability and as a result, a better traction between vehicle wheels and road surface.

The first goal is associated with reducing the amplitude of the vertical transferences and especially the vertical accelerations of the body mass of the vehicle. The second goal is associated with reducing the amplitude of the vertical displacements of vehicle's wheel mass and increasing the friction force.

The better comfort demands in principle a softer suspension, while the higher stability of the vehicle needs a harder suspension. On the other hand, decreasing the amplitude of vertical transferences of the vehicle body does not correlate equivalently with acceleration decrease. The passive approach at solving the problem is limited. Good results are achieved with semi-active suspension which does not add the energy to the system, but allows a continuous variation of the rate of energy dissipation using electro or magneto-rheological type dampers. The damping characteristic can be changed into certain limits by electro or magnet fields. These type vibro-protecting systems are sparing and reliable. A comparative analysis between passive and semi-active type suspension systems is made in the current paper. Some control approaches are investigated, taking into consideration the influence of physical characteristics of the actuators and associated non-linear effects.

PASSIVE SUSPENSION ANALYSIS

For purpose of analysis and control of the semi-active suspension of the vehicle, good results can be obtained using quarter car model. A quarter car model is enough physically adequate and with its simplicity is very appropriate for real time control synthesis. The obtained results can be easily adapted to more complex models. It is shown on the Fig.1.

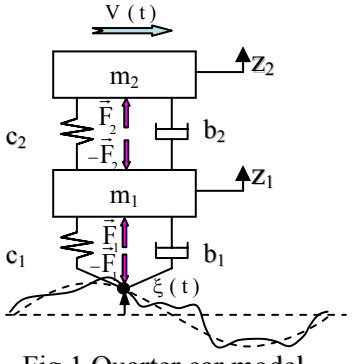

Fig.1 Quarter car model

The degrees of freedom are:
z_1 - the displacement in vertical direction of the unsprung vehicle elements, corresponding to one wheel;
z_2 – the respective displacement of the sprung masses.
The characteristics of the model are:
m_1, m_2 - the masses of the sprung and the unsprung vehicle elements;
c_1, c_2 - elastic coefficients of the tire and the suspension respectively;
b_1, b_2 - damping coefficients of the tire and the suspension respectively;

$V(t)$ - Velocity change; $\xi(t) = \xi_h(S(t)) + \xi_s(S(t))$ - a kinematical excitation from the road roughness, where: $S(t)=\int_{t_0}^{t} V(t)dt$ - The traveled distance; $\xi_h(t) = H_h * \sin(2\pi S(t)/L)$ a component of the kinematical excitation modeling the road roughness as a harmonic function with amplitude H_h and length of the wave L; $\xi_s(S(t))$ - a component of the kinematical excitation modeling the road roughness as a random function, presented as a process with normal distribution with zero mean value and deviation H_s.

The excitation ξ is generated for discrete values of S with samples ΔS (m), and the intermediate values necessary for the numerical simulation are calculated by spline interpolation. The derivative of ξ is calculated using mean differences: $\dot{\xi}(t) \approx [\xi(t+\Delta t) - \xi(t)]/\Delta t$, where the increment of the time Δt is set to 0,001 s; $\vec{F}_1$, $\vec{F}_2$ are the forces transmitted through the tire to unsprung mass and respectively from it to the sprung mass.

The differential system of equation describing the model is:

$m\ddot{q} + b\dot{q} + cq = dU$,
where:

$q = [z_1 \quad z_2]^T$, $U=[\xi \quad \dot{\xi}]^T$,

$m = \begin{bmatrix} m_1 & 0 \\ 0 & m_2 \end{bmatrix}$, $b = \begin{bmatrix} b_1 + b_2 & -b_2 \\ -b_2 & b_2 \end{bmatrix}$, $c = \begin{bmatrix} c_1 + c_2 & -c_2 \\ -c_2 & c_2 \end{bmatrix}$, $d = \begin{bmatrix} c_1 & b_2 \\ 0 & 0 \end{bmatrix}$,

^{T} – matrix transpose.

The state vector is:

$$X = [q \quad \dot{q}]^T = [z_1 \quad z_2 \quad \dot{z}_1 \quad \dot{z}_2]^T \tag{1}$$

and the output vector:

$$Y = [z_1 \quad z_2 \quad -F_i^d \quad \ddot{z}_2]^T, \tag{2}$$

where F_i^d is the dynamic normal component of the road interaction force.

The state-space presentation is obtained:

$$\dot{X} = AX + BU, \quad Y=CX+DU \tag{3}$$

where matrices of the state A and the external excitations B are:

$A = \begin{bmatrix} 0_{2x2} & I_2 \\ -m^{-1}c & -m^{-1}b \end{bmatrix}$, $B = \begin{bmatrix} 0_{2x2} \\ m^{-1}d \end{bmatrix}$,

and of the output variables are:

$C = \begin{bmatrix} I_2 & 0_{2x2} \\ c_1 & 0 & b_1 & 0 \\ c_2/m_2 & -c_2/m_2 & b_2/m_2 & -b_2/m_2 \end{bmatrix}$, $D = \begin{bmatrix} 0_{2x2} \\ -c_1 & -b_1 \\ 0 & 0 \end{bmatrix}$,

0_{2x2} – zero matrix 2x2, I_2 identical matrix.

The transfer function (TF) of the system is:

$$W^{(k)}(s) = \frac{\tilde{Y}}{\tilde{U}(k)} = \left[C(sI - A)^{-1} B + D(:,k) \right] = \frac{\operatorname{diag}\left\{ \begin{bmatrix} s^{m_1^{(k)}} & s^{m_1^{(k)}-1} & : & 1 \\ & & : & \\ s^{m_4^{(k)}} & s^{m_4^{(k)}-1} & : & 1 \end{bmatrix} \right\} \underbrace{\begin{bmatrix} b_{1,1}^{(k)} & b_{1,2}^{(k)} & .. & b_{1,m_1^{(k)}+1}^{(k)} \\ & & : & \\ b_{4,1}^{(k)} & b_{4,2}^{(k)} & .. & b_{4,m_1^{(k)}+1}^{(k)} \end{bmatrix}^T}_{Num^{(k)}}}{\underbrace{[1, a_2, a_3, a_4, a_5]}_{Den} [s^4, s^3, .., 1]^T}$$

where: $W^{(k)}$ - TF with respect to k input (k=1,2),
s is Laplace operator,
~ is the Laplace image sign,
diag{} is diagonal matrix with the elements of the argument on the diagonal,
$D(:,k)$ the k column of the matrix,
Den – matrix of the coefficients in the denominator of the TF,
$Num^{(k)}$ – matrix of the coefficients of the nominators of TF's between k input and output values;
$\left[m_1^{(k)},..,m_4^{(k)}\right]$, k=1,2 - matrix containing the rate of the nominators of the TF's.

Since the first input of the model (correspond to the elasticity of the tire) is the kinematical excitation and the second one (correspond to the damping of the tire) is it's derivative, these two inputs could be combined into one. Taking into account that $\dot{\tilde{\xi}} = s\tilde{\xi}$, for the TF with respect to i-output value is obtained:

$$W_i(s) = \left\{ Num^{(1)}(i,:) \left[s^{m_1^{(1)}}, s^{m_1^{(1)}-1}, .., 1 \right]^T + Num^{(2)}(i,:) \left[s^{m_1^{(2)}}, s^{m_1^{(2)}-1}, .., 1 \right]^T \right\} \frac{1}{Den\left[s^4, .., s^0 \right]}, i = 1,..,4 \quad (4)$$

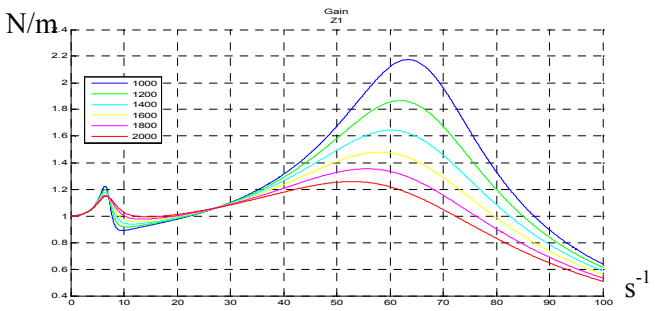

Fig. 2a. AFC

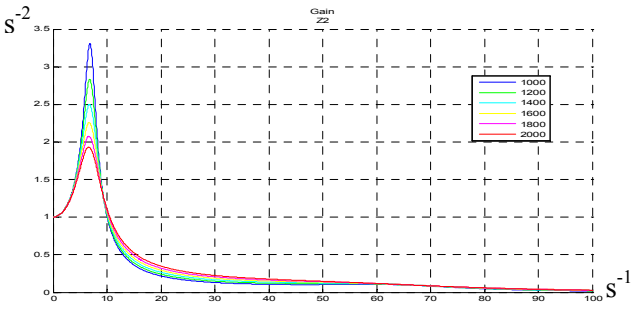

Fig. 2b. AFC

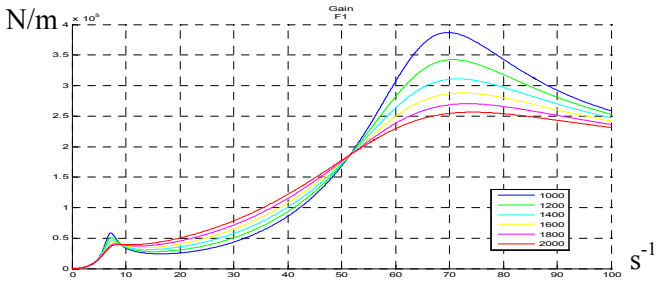

Fig. 2c. AFC

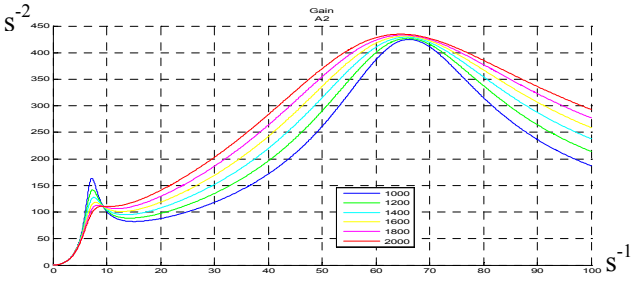

Fig. 2d. AFC

Amplitude/frequency characteristics are $A_i(p) = \left| W_i\left(s = p\sqrt{-1}\right) \right|$, i=1,..,4, where p is the angular frequency.

On the Fig.2a-d are shown the amplitude/frequency characteristics (AFC) towards Y - components, received with the following values of the system: m_1=40kg; c_1=1,6.10^5N/m; b_1=110Ns/m; m_2=350kg; c_2=0,19.10^5N/m; b_2=[1:0,2:2] kNs/m.

The analysis showed that lower levels of damping cause higher vibration amplitudes in the range of resonance frequencies. At the same time they decrease the dynamics into between-resonance zone and provide a better comfort in this range. So for restriction of resonance phenomena and for better stability of the vehicle at high frequencies (respectively at high speed) the high damper ratio is needed. On the other hand with purpose of reducing the dynamics into between-resonance zone and for better driving comfort, the damping ratio should be diminished. This contradiction can be explained by the fact that due to phase shifting during the part of oscillation period the damper force has the same direction with the velocity of the body mass or to the wheel mass. In these periods instead to dissipate the energy, the damper directs it either to the body mass or to the wheel mass. This effect is more essential into between-resonance zone.

With the output variables' matrices - $C1 = \begin{bmatrix} 0_{2x2} & I_2 \\ 0_{2x2} & \begin{matrix} -1 & 1 \\ 1 & -1 \end{matrix} \end{bmatrix}$, $D1 = 0_{4x2}$,

are obtained the TF-s with respect to the velocities $W_{\dot{z}_1} = \dot{\tilde{z}}_1/\tilde{\xi}$ и $W_{\dot{z}_2} = \dot{\tilde{z}}_2/\tilde{\xi}$ (after some transformations):

$$W_{\dot{z}_1/(\dot{z}_2-\dot{z}_1)} = \frac{\dot{\tilde{z}}_1}{(\dot{\tilde{z}}_2 - \dot{\tilde{z}}_1)} = \frac{(m_2 s^2 + b_2 s + c_2)}{-m_2 s^2}, \quad W_{\dot{z}_2/(\dot{z}_1-\dot{z}_2)} = \frac{\dot{\tilde{z}}_2}{(\dot{\tilde{z}}_1 - \dot{\tilde{z}}_2)} = \frac{(b_2 s + c_2)}{m_2 s^2}. \qquad (5)$$

Phase/frequency characteristics (PFC) $\Phi(p) = \mathrm{Arg}\left[W\left(s = p\sqrt{-1}\right) \right]$ for (5) are:

$$\Phi_{\dot{z}_1/(\dot{z}_2-\dot{z}_1)}(p) = \mathrm{atan}\left(\frac{b_2 p}{c_1 - m_2 p^2}\right) = \begin{cases} 0, \text{ за } p=0 \\ \pi, \text{ за } p \Rightarrow \infty \end{cases}, \quad \Phi_{\dot{z}_2/(\dot{z}_1-\dot{z}_2)}(p) = \mathrm{atan}\left(\frac{b_2 p}{c_1}\right) - \pi = \begin{cases} -\pi \text{ или } \pi, \text{ за } p=0 \\ -\frac{\pi}{2} \text{ или } \frac{3}{2}\pi, \text{ за } p \Rightarrow \infty \end{cases}.$$

They are shown on the Fig. 3a-b.

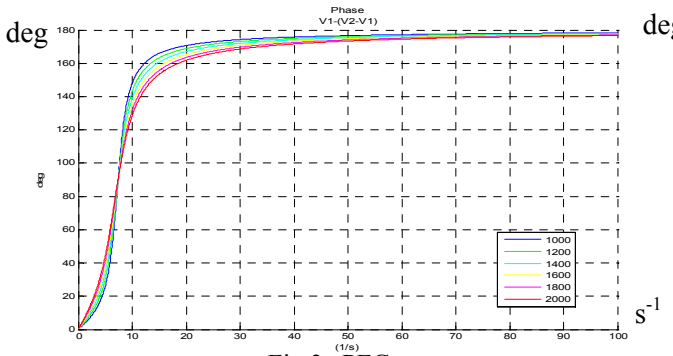

Fig.3a PFC

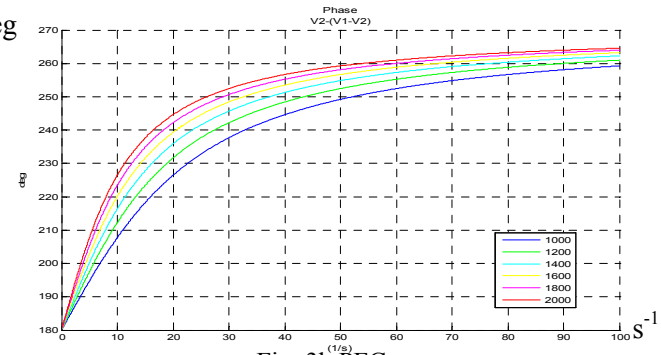

Fig. 3b PFC

As shown in the Figs. 3a and 3b, disturbance frequencies into the direction of the damper force are nearly opposed to the direction of the speed of body mass, but with

increasing the frequencies this state is changed and duration of the periods when the forces act in the same direction is increased as well. For wheel mass, at low frequencies the force into damper has the same direction (phase) during longer part of the period of oscillation. At high frequencies, the vibration transferences at the body mass are decreasing and the force into the damper is opposed to the movement direction of the wheel mass.

Figures 4a and 4b show the time simulation results concerning correlation between movement direction of the mass and direction of the force from damper acting on them. The diagrams show up the periods when both directions coincide and the damper directed energy to the corresponding mass.

Results from the modeling, for different values of damping coefficients are shown in Reference Table. The characteristics of the kinematical excitation are: H_h=0,015m, L=7m, H_s=0,005m, ΔS=0,35m. The motion is with acceleration a=1,1 m/s^2 to the maximal velocity V_{max}=130km/h, and after this is established to uniform motion. The simulation period is T_k=35s.

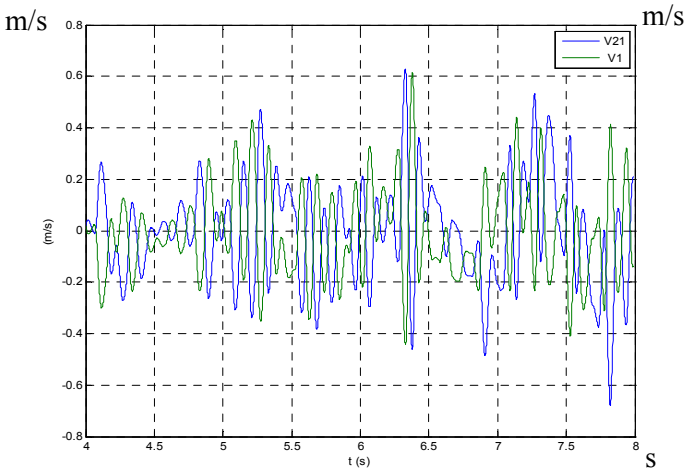

Fig. 4a. Velocity comparison

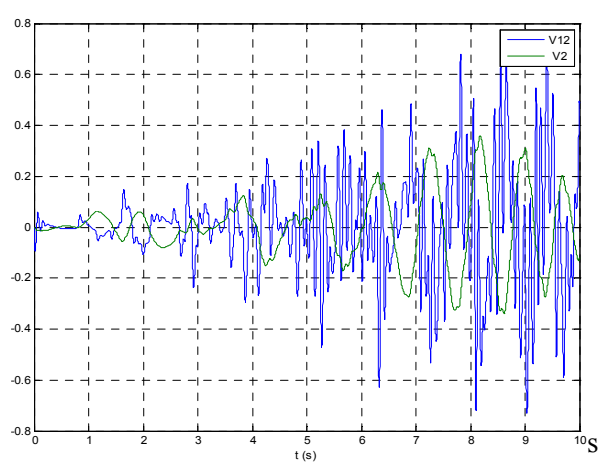

Fig. 4b. Velocity comparison

In the Reference Table with RMS is denoted the root mean square value of the argument $RMS(u)=\sqrt{\frac{1}{T_k}\int_0^{T_k}\|u(t)\|^2 dt}$, and the maximal value $Max(|u|)=\max_{t\in[0,T_k]}|u(t)|$.

According to the analysis results, the increasing of the suspension damping coefficient b_2 lead to:

- the resonance itself is decreasing and the transference of both masses;
- the acceleration of the sprung mass increases, and for the unsprung one - decreases;
- the dynamic tangent component F_1^d of the road interaction force decreases to a specified value of b_2 (respectively the stability), after this it begins to increase again;

All these conclusions are confirmed from the amplitude/frequency characteristics from Fig. 2.

NATURE OF SEMI-ACTIVE CONTROL AND CONTROL LAWS

The problem with the upper contradictory influence of the damping coefficient could be solved by using semi-active dampers. Due to the change of a magnetic or electric field their damping coefficients vary between lower and upper boundaries $b_2 \in \left[b_2^l, b_2^u \right]$. In the ideal model of this type of damping devices, the alteration of the damping coefficient is a linear function of the control signal (for MR dampers this is the current $i \in [0, i_{max}]$):

$$b_2 = b_2^l + (b_2^u - b_2^l)\frac{i}{i_{max}} \tag{6}$$

When the main objective is increasing of the riding comfort and the damper force acts in same direction with sprung mass movement the control signal is zero and the damping coefficient receives its minimal value:

$$\dot{z}_2 \left(\dot{z}_1 - \dot{z}_2 \right) \geq 0 \Rightarrow i = 0 \Rightarrow b_2 = b_2^l \tag{7}$$

This control type is known in the literature as “Skyhook”. When the main objective is increasing of the vehicle stability and the damper force acts in same direction with unsprung mass movement the control is:

$$\dot{z}_1 \left(\dot{z}_2 - \dot{z}_1 \right) \geq 0 \Rightarrow i = 0 \Rightarrow b_2 = b_2^l \tag{8}$$

This control type is known in the literature as „Groundhook”.

The “Hybrid” (compromise) logic would take the following form:

$$\begin{vmatrix} \dot{z}_2(-\dot{z}_2 + \dot{z}_1) \geq 0 \cap \dot{z}_1(\dot{z}_2 - \dot{z}_1) \geq 0 & \Rightarrow i = i_{off} = 0, \\ \dot{z}_2(-\dot{z}_2 + \dot{z}_1) < 0 \cap \dot{z}_1(\dot{z}_2 - \dot{z}_1) \geq 0 & \Rightarrow i = \alpha i_{on}, \\ \dot{z}_2(-\dot{z}_2 + \dot{z}_1) \geq 0 \cap \dot{z}_1(\dot{z}_2 - \dot{z}_1) < 0 & \Rightarrow i = (1-\alpha) i_{on}, \\ \dot{z}_2(-\dot{z}_2 + \dot{z}_1) \leq 0 \cap \dot{z}_1(\dot{z}_2 - \dot{z}_1) \leq 0 & \Rightarrow i = i_{on}, \\ \alpha \in [0,1] \end{vmatrix} \tag{9}$$

where i_{on} is the on state control current, α is the compromise factor.

This logic embraces the other two types of control - when α=1 the control will be Skyhook, analogically when α=0 – Groundhook control. The optimal value for α is determined by multi-criteria optimal synthesis [Genov J., 2004].

Semi-Active Controllers

Discrete “On – Off” controller The control signal i takes only two values: 0 or i_{max}. According to the logic (9), the damping coefficient takes discrete value and the control law is:

$$\begin{vmatrix} \dot{z}_2(-\dot{z}_2 + \dot{z}_1) \geq 0 \cap \dot{z}_1(\dot{z}_2 - \dot{z}_1) \geq 0 & \Rightarrow i = 0, \quad b_2 = b_2^l \\ \dot{z}_2(-\dot{z}_2 + \dot{z}_1) < 0 \cap \dot{z}_1(\dot{z}_2 - \dot{z}_1) \geq 0 & \Rightarrow i = i_{max}, b_2 = b_2^l + (b_2^u - b_2^l)\alpha \\ \dot{z}_2(-\dot{z}_2 + \dot{z}_1) \geq 0 \cap \dot{z}_1(\dot{z}_2 - \dot{z}_1) < 0 & \Rightarrow i = i_{max}, b_2 = b_2^l + (b_2^u - b_2^l)(1-\alpha) \\ \dot{z}_2(-\dot{z}_2 + \dot{z}_1) \leq 0 \cap \dot{z}_1(\dot{z}_2 - \dot{z}_1) \leq 0 & \Rightarrow i = i_{max}, b_2 = b_2^u \\ \alpha \in [0,1] \end{vmatrix} \tag{10}$$

The structure of On-Off controller is represented in the environment of MatLab – Simulink – Fig. 5. The results of the numerical simulation for b_l=780, b_u=2230 Ns/m are shown in Reference Table.

Comparing the results with these in Reference Table, for passive insulation, shows the effectiveness of semi-active control. The reduction of the transference of the sprung mass during Skyhook control is almost double. Analogically for the unsprung mass, the results are also better. Main disadvantage is the small increasing of the acceleration of the upper (sprung) mass. This negative effect is caused by the fast switching of the damping coefficient, equivalent to internal impacts for the system.

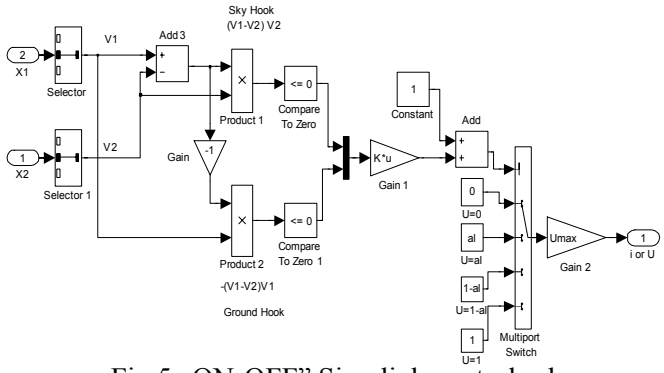

Fig.5 „ON-OFF" Simulink control scheme

Continuous control law proportional to the absolute velocity (Vabs controller)

These controllers aim to decrease the negative effect during fast switching. For this type the idea is to emulate a damper hooked in a fictional point in the sky:

$$F_2^s = \left[b_2^l + (b_2^u - b_2^l)\frac{i^s}{i_{max}} \right](\dot{x}_1 - \dot{x}_2) = -K_s b_2^u \dot{x}_2 ,$$

and for Groundhook:

$$-F_2^g = \left[b_2^l + (b_2^u - b_2^l)\frac{i^g}{i_{max}} \right](\dot{x}_2 - \dot{x}_1) = -K_g b_2^u \dot{x}_1 ,$$

where K_s and K_g are the emulation coefficient. From the upper case, the control signal is:

$$i^{s/g} = \frac{i_{max}}{b_2^u - b_2^l}\left(K_{s/g}\frac{\dot{x}_2}{\dot{x}_2 - \dot{x}_1} b_2^u - b_2^l \right).$$

Physically the nature of the semi-active suspension control lays is limited by requirement $i \in [0, i_{max}]$, which is transformed into: $\frac{\dot{x}_2}{\dot{x}_2 - \dot{x}_1} \in \frac{1}{K_{s/g}}\left[\frac{b_2^l}{b_2^u}, 1 \right]$. So for the generalized Hybrid control logic:

$$
\begin{aligned}
&\dot{z}_2(-\dot{z}_2+\dot{z}_1)>0 \cap \dot{z}_1(\dot{z}_2-\dot{z}_1)>0 \quad \Rightarrow i=0,\ b_2=b_2^l;\\
&\dot{z}_2(-\dot{z}_2+\dot{z}_1)\le 0 \cap \dot{z}_1(\dot{z}_2-\dot{z}_1)>0 \quad \Rightarrow \begin{cases} F_2=\alpha F_2^s \\ i=i^s=\dfrac{i_{max}\alpha}{b_2^u-b_2^l}\left(K_s\dfrac{\dot{x}_2}{\dot{x}_2-\dot{x}_1}b_2^u-b_2^l\right); \\ b_2=b_2^l+\alpha\left(K_s\dfrac{\dot{x}_2}{\dot{x}_2-\dot{x}_1}b_2^u-b_2^l\right)\end{cases}\\
&\dot{z}_2(-\dot{z}_2+\dot{z}_1)>0 \cap \dot{z}_1(\dot{z}_2-\dot{z}_1)\le 0 \quad \Rightarrow \begin{cases} F_2=(\alpha-1)F_2^g \\ i=i^g=\dfrac{i_{max}(1-\alpha)}{b_2^u-b_2^l}\left(K_g\dfrac{\dot{x}_1}{\dot{x}_1-\dot{x}_2}b_2^u-b_2^l\right); \\ b_2=b_2^l+(1-\alpha)\left(K_g\dfrac{\dot{x}_1}{\dot{x}_1-\dot{x}_2}b_2^u-b_2^l\right)\end{cases}
\end{aligned}
\tag{11}
$$

$$
\dot{z}_2(-\dot{z}_2+\dot{z}_1)\le 0 \cap \dot{z}_1(\dot{z}_2-\dot{z}_1)\le 0 \Rightarrow \begin{cases} F_2=\alpha F_2^s+(\alpha-1)F_2^g \\ i=i^s+i^g=\dfrac{i_{max}}{b_2^u-b_2^l}\left(\dfrac{\alpha K_s\dot{x}_2-(1-\alpha)K_g\dot{x}_1}{\dot{x}_2-\dot{x}_1}b_2^u-b_2^l\right); \\ b_2=b_2^l+\left(\dfrac{\alpha K_s\dot{x}_2-(1-\alpha)K_g\dot{x}_1}{\dot{x}_2-\dot{x}_1}b_2^u-b_2^l\right)\end{cases}
$$

$$
\begin{aligned}
&i<0 \quad \Rightarrow i=0, \quad b_2=b_2^l;\\
&i>i_{max} \Rightarrow i=i_{max},\ b_2=b_2^u;\\
&\alpha\in[0,1].
\end{aligned}
$$

The emulation coefficients K_s and K_g define the dynamics of control. Increasing the values of the coefficients, this control type will correspond to the discrete one, lowering will limit the functionality of the damper. So an optimization procedure is suggested to define the best values for K_s and K_g.

We suggest an optimizing modification of this control:

$$
\begin{aligned}
&\dot{z}_2(-\dot{z}_2+\dot{z}_1)>0 \cap \dot{z}_1(\dot{z}_2-\dot{z}_1)>0 \quad \Rightarrow i=0,\\
&\dot{z}_2(-\dot{z}_2+\dot{z}_1)\le 0 \cap \dot{z}_1(\dot{z}_2-\dot{z}_1)>0 \quad \Rightarrow i'=i^{s'}=\begin{cases} i^s & \text{, за } \dot{z}_2\ddot{z}_2\le 0 \\ i^s\left(1+\dfrac{K_2|\ddot{z}_2|}{\ddot{z}_2^{max}}\right) & \text{, за } \dot{z}_2\ddot{z}_2>0\end{cases},\\
&\dot{z}_2(-\dot{z}_2+\dot{z}_1)>0 \cap \dot{z}_1(\dot{z}_2-\dot{z}_1)\le 0 \quad \Rightarrow i'=i^{g'}=\begin{cases} i^g & \text{, за } \dot{z}_1\ddot{z}_1\le 0 \\ i^g\left(1+\dfrac{K_1|\ddot{z}_1|}{\ddot{z}_1^{max}}\right) & \text{, за } \dot{z}_1\ddot{z}_1>0\end{cases},\\
&\dot{z}_2(-\dot{z}_2+\dot{z}_1)\le 0 \cap \dot{z}_1(\dot{z}_2-\dot{z}_1)\le 0 \quad \Rightarrow i'=\alpha i^{s'}+(1-\alpha)i^{g'}\\
&\alpha\in[0,1],\ i'\in[0,i_{max}],\ \tilde{i}=\frac{1}{T_f s+1}\tilde{i'}.
\end{aligned}
\tag{12}
$$

In (12), i_s and i_g are calculated according the dependencies (11). The main idea is to force the control in cases of fast velocity change.

For preventing the fast switches on the regulator output is added, a first order filter with time-constant - T_f and TF - $W_f(s)=\dfrac{1}{T_f s+1}$. The results for K_1=4, K_2=10, $\ddot{z}_1^{max}$=50 m/s^2, $\ddot{z}_2^{max}$=6 m/s^2 are shown in Reference Table. They are better than the Vabs ones – except the road interaction force.

PID controller The suggested control logic is:

$$
\begin{aligned}
&\dot z_2(-\dot z_2+\dot z_1)\ge 0 \cap \dot z_1(\dot z_2-\dot z_1)\ge 0 && \Rightarrow i=0,\\
&\dot z_2(-\dot z_2+\dot z_1)< 0 \cap \dot z_1(\dot z_2-\dot z_1)\ge 0 && \Rightarrow i^s=\left|K_I^s\frac{z_2}{z_2^{max}}+K_P^s\frac{\dot z_2}{\dot z_2^{max}}+K_D^s\frac{\ddot z_2}{\ddot z_2^{max}}\right|\alpha,\\
&\dot z_2(-\dot z_2+\dot z_1)\ge 0 \cap \dot z_1(\dot z_2-\dot z_1)< 0 && \Rightarrow i^g=\left|K_I^g\frac{z_1}{z_1^{max}}+K_P^g\frac{\dot z_1}{\dot z_1^{max}}+K_D^g\frac{\ddot z_1}{\ddot z_1^{max}}\right|(1-\alpha),\\
&\dot z_2(-\dot z_2+\dot z_1)\le 0 \cap \dot z_1(\dot z_2-\dot z_1)\le 0 && \Rightarrow i=i^s+i^g,\\
&i\in[0,i_{max}];\alpha\in[0,1]
\end{aligned}
\qquad (13)
$$

Here $z_1^{max},\dot z_1^{max},\ddot z_1^{max}$ и $z_2^{max},\dot z_2^{max},\ddot z_2^{max}$ are the absolute maximal values which are used to norm the signals, and K_I^s, K_P^s, K_D^s, и K_I^g, K_P^g, K_D^g are the coefficients of the PID controller.

In Reference Table are shown the results from the modeling. The analysis shows better results than Vabs controller during Groundhook and Hybrid control, but there is insignificant increasing of the sprung mass acceleration.

PHYSICAL AND MECHANO-MATHEMICAL MODEL OF THE SEMI-ACTIVE DAMPER

Physical Basis of the Behavior of the MR and ER Fluids

MR and ER fluids are suspensions comprising some base fluid (most often silicon oil) and electro-polarized or respectively magnet-polarized particles, some micrometers in size. The fluids include also some ingredients aimed at decreasing the solidification, stratification, precipitation and other alterations with time.

The dampers using MR fluid create greater force in comparison with dampers with ER fluid. The monitoring magnetic field of this type of damper is generated easier and they are less sensitive to contamination. The magnetic moment $\vec p_m$ of the electron q, rotating with velocity v, along trajectory with radius r is $p_m=0{,}5qvr$. The magnetic moment is oriented in opposite direction of the kinetic momentum $\vec K$.

When magnetic field with magnetic inductance $\vec B$ is applied, a force $\vec f_m=q\vec v\times\vec B$ acts upon the electrical charge Fig.6. So mechanical moment acting upon two opposite electrical charges and which orients the dipoles according to the direction of the magnetic fields is equal to:

$$\vec M_m=2\vec r\times\vec f_m=2\vec r\times q\vec v\times\vec B=\vec p_m\times\vec B.$$

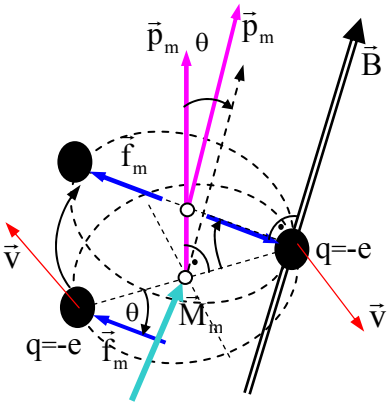

Fig.6 Magnetic field action

Quantitative characteristic of the magnetizing of the substance (fluid) is represented by the vector of magnetization, calculated as a sum of the magnetic moments per unit volume $\vec P_m=\sum_V\vec p_{m_i}\Big/V$, Am^{-1}.

According to the quantum mechanics, the module of the vector of magnetization in presence of n_m magnetic dipoles per unit volume is equal to

$$P_m = n_m p_m = n_m p_l \mathrm{th}\left(p_l B/kT\right) \qquad (14)$$

where: k, J/K– Boltzmann constant; T- temperature in ^{0}K; p_1- magnetic momentum, characterizing the spin of the electron along it's axis. When external magnetic field is applied, the induction of the local magnetic fields, acting upon the spin magnetic momentums is:

$$B = B_0 + B_{ind} \qquad (15)$$

where $B_0=\mu_0 H$ is the magnetic inductance of the external field and $B_{ind} = \lambda\mu_0 P_m$ of induced field (μ_0 is vacuum permeability, λ is a constant, assessed magnetic interaction between atoms).

After substitution in (14) is received nonlinear equation:

$$P_m = n_m p_l \mathrm{th}\left[p_l\left(B_0 + \lambda\mu_0 P_m\right)/kT\right] \qquad (16)$$

From the first Maxwell equation comes that the intensity of the magnetic field is:

$$\vec{H} = \mu_0^{-1}\vec{B} - \vec{P}_m, \mathrm{Am}^{-1} \qquad (17)$$

In the upper equation magnetic induction is substituted to zero, $P_m = P_m^r \neq 0$ i.e. for zero intensity the domains do not return into their initial condition and they retain the orientation with remaining induction $B_r = \mu_0 P_m^r$. For zero reduction of this remaining induction an external field with opposite direction is needed H_c.

The increasing of B_0 originates a saturation i.e. $P_m \Rightarrow n_m p_1$. This effect comes from the increasing continues to lengths of $10^{-3}\div10^{-5}$ mm and the amount of the atoms in it is $10^6\div10^9$. After this due to the external parallel orientation that do not coincide with the ferrite crystals axes, the increasing ceases. A microscope photo of the formed domains is shown on Fig. 7. The dependencies (16) and (17) are nonlinear and influent from the magnetic history (hysteresis) Fig.8.

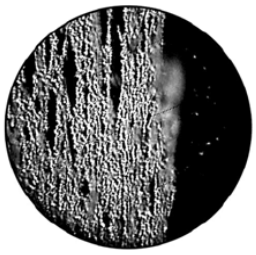

Fig.7. Microscope photo of MR fluid

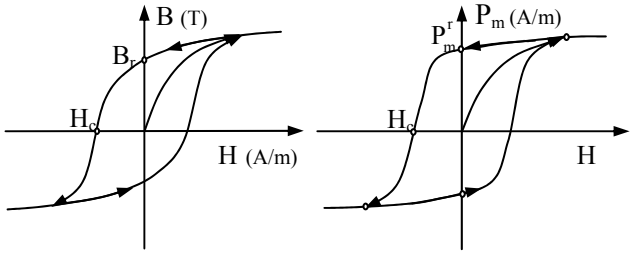

Fig.8. Magnetic responses of MR fluid

Mechano-Mathemical Model of the MR Damper

The above mentioned paragraph demonstrates that some non-linear effects in characteristic of the MR damper exist. When shearing effort is applied and shearing stress is smaller then the value τ_y when the domains are torn, the fluid becomes plastic. If the value of the shearing stress become higher than τ_y, the fluid becomes

viscose. The shearing stress τ_y, up to one specific value is in quadratic dependence of the intensity H. The characteristic of the MR damper up to value of the force, corresponding with τ_y has the same form dependence as $P_m(H)$. Above this value, the characteristic becomes linear.

Newton accepted that for laminar flow of fluid between two surfaces with linear gradient of speed, the shearing stress is proportional to the gradient of the velocity $\tau = \eta_p \frac{\partial v}{\partial y} = \eta_p \dot{\gamma}$. This describes the model of the linear damper.

Plastic model of Bingham [3]

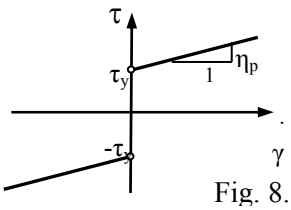

$$\begin{cases} \dot{\gamma} = 0 & ,|\tau| < \tau_y \\ \tau = \tau_y \text{sign}(\dot{\gamma}) + \eta_p \dot{\gamma} & ,|\tau| \geq \tau_y \end{cases}$$

Fig. 8. Bingham model

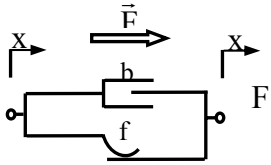

$$F = b(\dot{x}_1 - \dot{x}_2) + f_c \text{sign}(\dot{x}_1 - \dot{x}_2)$$

Fig.9. Bingham mechanical presentation

This model (Fig. 8) is fundamental when behavior of the rheological fluids is described. It was proposed for the first time by Philips R.W. in 1969.

According to this model the force into the damper can be accepted as a result of combination of a parallel acting viscose damper and damper with a constant value of the force of dry friction f_c - Fig.9. A disadvantage of the model is that for values of the stress less than τ_y it does not take in account the relevant elastic deformation, slipping between dipole chains and hysteresis during magnetizing and formation of the domains.

Modified model of Bouc – Wen – Spencer (BWS) [1]

This model is based on approximation of the hysteresis characteristic, propounded by Wen, Y., 1976. The mechanical analogue of this model is shown on Fig. 10.

This model takes into account the presence of linear damping ratio b_0 and elasticity c_0 of the damper with the hydro-accumulator and a hysteresis at low speed of deformation. For better dynamics description, there are included an additional damper with coefficient b_0^* and parallel elastic element with coefficient c_0^*.

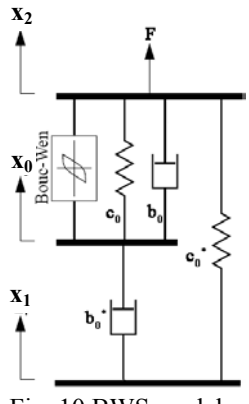

Fig. 10 BWS model

The damper force is:

$$F = c_0(x_0 - x_2) + b_0(\dot{x}_0 - \dot{x}_2) - c_h\zeta + c_0^*(x_1 - x_2 + \delta_0) = c_0^*(x_1 - x_2 + \delta_0) - b_0^*(\dot{x}_0 - \dot{x}_1), \quad (18a)$$

Where: c_h N/m - reduced elasticity coefficient bounded to the characteristics slope change; δ_0 - presence of hydraulic accumulator. From the force balance on x_0, follows:

$$\dot{x}_0 = \left[b_0^* \dot{x}_1 + b_0 \dot{x}_2 - c_0(x_0 - x_2) + c_h\zeta \right] / (b_0 + b_0^*). \quad (18b)$$

The evolutionary variable is obtained from equation:

$$\dot{\zeta} = -\gamma|\dot{x}_0 - \dot{x}_2|\zeta|\zeta|^{\chi-1} + \beta(\dot{x}_0 - \dot{x}_2)|\zeta|^{\chi} - \nu(\dot{x}_0 - \dot{x}_2) = \left\{\left[\beta - \text{sign}\left((\dot{x}_0 - \dot{x}_2)\zeta\right)\gamma\right]|\zeta|^{\chi} - \nu\right\}(\dot{x}_0 - \dot{x}_2), \quad (18c)$$

where γ, β, ρ and χ are hysteresis form coefficients.

The characteristics of the model depend on the magnetic field alternation, respectively from the control current i. The values of c_h, b_0 and b_0^*, in first approximation there are presented the following linear dependencies:

$$c_h = c_h^c + c_h^v i', \; b_0 = b_0^c + b_0^v i', \; b_0^* = b_0^{*c} + b_0^{*v} i' \quad (18d)$$

Here i' is a function rendering the process of the rheological equilibrium:

$$\dot{i}' = \left(i - i'\right)/\tau_r, \quad (18e)$$

where: i – control current, τ_r – time constant of the process.

Fig. 11 MR Damper of LORD Corporation

Table 1. BWS model parameters

b_0^c, Ns/m	b_0^V, Ns/mA	c_0, N/m	c_h^c, N/m	c_h^V, N/mA
780	2230	1400	14500	71500
b_0^{*c}, Ns/m	b_0^{*V}, Ns/mA	c_0^*, N/m	χ	τ_r, s
28000	500	540	2	0,0053
γ, m^{-2}	β, m^{-2}	δ	δ_0, m	
$0{,}5\ 10^6$	$0{,}8\ 10^6$	170	0	

The parameters of the model were identified for MR damper of „LORD Corporation"-USA RD-1005-3 - Fig.11. After numerical solution of the optimization using least squares, were identified the parameter values of the model Table 1.

Model of the Control Electrical Chain of MR Damper, Fig.12

Here R is the active resistance of the control coil and the supply cable; L – inductivity of the control coil; U_0 – supply voltage; U_{contr}- control voltage. The control current is defined by the following equation:

$$L\frac{di}{dt} + Ri = U_{out}(t) = \begin{cases} U_0, \text{за } (t \bmod T_m) \le T_{on} \\ 0 \;\; , \text{за } (t \bmod T_m) > T_{on} \end{cases} \quad (19)$$

$$i(0) = 0$$

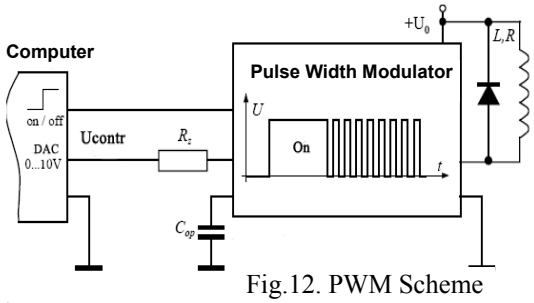

Fig.12. PWM Scheme

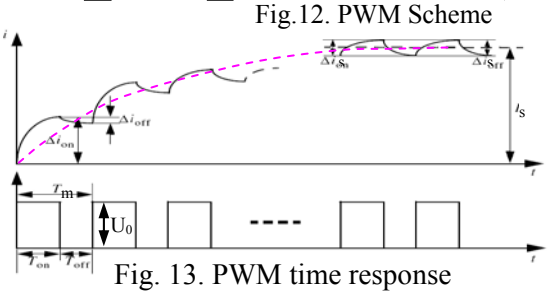

Fig. 13. PWM time response

where: T_m is the modulation period, $T_{on} = K_M U_{contr}$ current sample for T_m, $K_M = K_{wpm} R T_m / U_0$, K_{wpm} - gain of pulse width modulator (PWM). The solution of (21) is shown on Fig. 13.

The big value of the modulation frequency $f_m=T_m^{-1}$ demands only a very small integration sample for the numerical modeling. Approximation model with transfer function is more convenient to be used:

$$W(s) = \frac{\tilde{i}}{\tilde{U}_{contr}} = \frac{K_{wpm}}{(\underbrace{L/R}_{\tau_u})s + 1} \qquad (20)$$

The amplifier has an insensitiveness zone $U_{contr}<U_d$. The used PWM signal magnifier of "LORD Corporation" RD-3002-03, K_{wpm}=0,4 A/v, U_d=0,5 v. The control chain of RD-1005-3 has R=4Ω and L=0,0543 H.

The time-constant of (22) is too big, and this leads to significant alteration of the control signal, as it is shown on Fig.14. For this problem reducing a PID-regulator feed back is exploit Fig.15. The parameters of the regulator are K_fb=1/0,401 vA^{-1} (it is from the order of $1/K_{wpm}$), K_p=15, K_i=5, K_d=8, T_d=1s, U_{max}=±5v.

As it could be seen on Fig. 14, there is a great improvement of the signal.

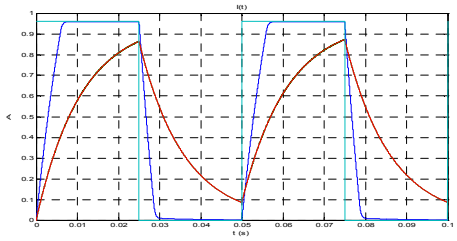

Fig.14. PWM responses vs. PID correction

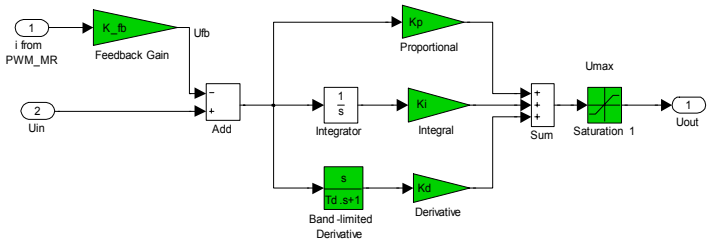

Fig. 15. PID Corrector -Simulink model

SEMI-ACTIVE CONTROL WITH GIVING AN ACCOUNT ON THE MR CHARACTERISTICS

Influence of the damper characteristics upon the semi-active control

The results are shown in Reference Table. The transferences are near to these of the linear damper, but the acceleration of the sprung mass and the dynamic friction force increase significantly. Similar change for worse of the quality criteria of the semi-active suspension is observed on the other controllers.

Semi-active control with giving an account on the MR characteristics

In order to reduce this negative effect, to the controllers is added a model of linear semi-active damper and its inverse model. The model (3) can be represented as:

$$\dot{X} = A'X + BU + RF_2, \quad Y = C'X + DU + GF_2 \qquad (21)$$

where A' is calculated for $b = b' = \begin{bmatrix} b_1 & 0 \\ 0 & 0 \end{bmatrix}$, $R = [0_{1x2}, -1, 1]^T$, $C' = C_{for\ b_2=0}$, $G = [0_{1x3}, 1]$.

Principle scheme of the control is shown on the Fig. 16.

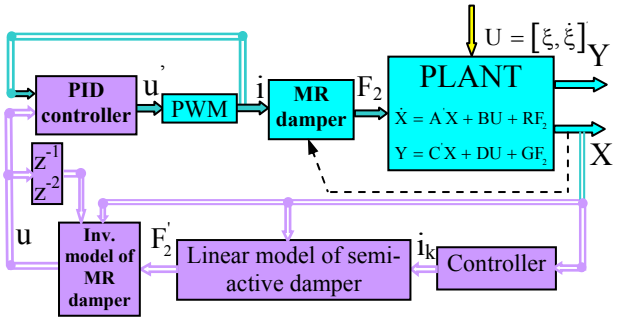

Fig.16. Block control diagram

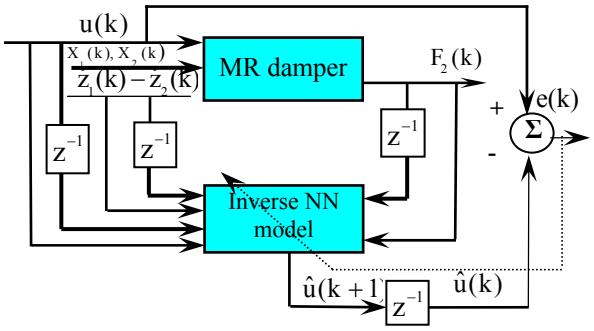

Fig.17 Training procedure

A basic feature of the algorithm is developing an inverse MR damper model. The strong nonlinearity of this model leads to analytical representation, which is impossible to be used in real-time applications. Thus here is applied an artificial neural network model of the damper.

For identification the inverse neural network model is used three layer cascade network with m, q и s neurons respectively in the first, second and the third layer. The activation function of the first and the second layer is $g_1(x)=g_2(x)=\frac{2}{1+e^{-2x}}-1$ and liner function for the third (output) layer $g_3(x)=x$. For the used model m=6, q=12 и s=1.

The weight coefficients are obtained by minimization of the error function using standard back propagation and Levenberg-Marquardt algorithm. For the discussed NN model identification of the input data vector is:

$$P(k)=[\,(\dot{z}_1(k)-\dot{z}_2(k)),\,(\dot{z}_1(k-1)-\dot{z}_2(k-1)),\,F_2(k),\,F_2(k-1),\,u(k),\,u(k-1)]^T,\ k=1,..,N \qquad (22)$$

k is number of time discrete. The output is the control voltage $\hat{u}(k+1),\ k=2,..(N-1)$.
The target is the referent control voltage is u(k+1), k=2,...,(N-1). Input and target signals are obtained by numerical simulation with BWS-model of the damper. The NN training scheme is shown on Fig.17.

During the simulation of already trained neural network is initiated external recursion. For the purpose the input data u(k) and u(k-1) are replaced by $\hat{u}(k)$ и $\hat{u}(k-1)$ from the network output. The effectiveness of the suggested approach is illustrated with On-Off controller “Skyhook” type Reference Table. The authors considered that there is not necessary to illustrate the effectiveness of the NN modeling with “groundhook” and “hybrid” control laws. This suggestion is made because by the analogy of the above mentioned analysis of the differences between the control laws. This step may be included into future development of a laboratory test bench.

As it could be seen from the Reference Table, the NN model of the MR damper suspension gives very good results near to an ideal damper. There is also another big advantage of NN based models and respectively control – the computational time. The time for solving the equations of MR damper, after taking into account the phenomenological BWS model, is very long. The analogical NN approximation of the plant model takes several seconds for computation. This is important point when analyzing data set in real time and building a real time control scheme for a test bench.

Such test bench was build and a demonstration of the suggested approach is ready to be shown.

REFERENCES

[1] Dyke, S.J., Spencer B.F. Jr., Sain M.K. and. Carlson J.D, “Seismic Response Reduction Using Magnetorheological Dampers”, Proceedings of the IFAC World Congress, San Francisco, California (1996).
[2] Jansen, L., Dyke, S., “Semi-Active Control Strategies for MR Dampers: A Comparative Study”, ASCE Journal of Engineering Mechanics, Vol. 126, No. 8, pp.795–803 (1999).
[3] Peschel, J., Roschke, P., “Neuro-Fuzzy model of a Large Magneto-rheological Damper”, Proceedings of Texas Section American Society of Civil Engineers – Spring Meeting, San Antonio March (2001).
[4] Genov J., Arnaudov K., Venkov G., “Optimal design of suspension with determinated and random kinematical excitations. Part 2 – optimal synthesis of semi-active suspension”, “Dynamic of machines”, № 50, pp.96-101,TU-Varna (2004).

REFERENCE TABLE

CHARACTERISTICS	Z_1	Z_2	Z_1	Z_2	Z_1	Z_2	Z_1	Z_2	Z_1	Z_2
	Passive b_2=780Ns/m		**"Skyhook" control On-Off**		**"Skyhook" control Vabs; K_s=2**		**"Skyhook" PID; K_s=1,4**		**MR "Skyhook" control OnOf**	
$\int_0^{T_1} Z(t)dt$	0,348	0,256	0,37	0,176	0,35	0,18	0,35	0,188	0,42	0,18
Max([Z, Ż, Z̈])	[0,03;1,42;97,1]	[0,055;0,42;3,89]	[0,03;1,11;78]	[0,026;0,19;5,8]	[0,03;1,4;98]	[0,027;0,21;3,8]	[0,03;1,3;92,3]	[0,027;0,2;6,41]	[0,03;1,37;106]	[0,021;0,2;8,2]
RMS([Z, Ż, Z̈])	[0,012;0,35;21,3]	[0,013;0,093;1,2]	[0,012;0,32;17,7]	[0,007;0,062;1,4]	[0,0117;0,35;21]	[0,0078;0,06;1,09]	[0,0118;0,33;19,6]	[0,008;0,064;1,19]	[0,014;0,34;17,2]	[0,006;0,09;2,4]
$RMS(F_1^d)$	852,4	-	850	-	844	-	823	-	1135	-
	Passive b_2=1505Ns/m		**"Hybrid" control On-Off, α=0,5**		**"Hybrid" Vabs α=0,5 K_s=2, K_g=1,4**		**"Hybrid" PID; α=0,5, K_s=1,4, K_g=1,4**		**MR "Hybrid" control On-Off, α=0,5**	
$\int_0^{T_1} Z(t)dt$	0,346	0,23	0,36	0,216	0,35	0,23	0,34	0,22	0,4	0,29
Max([Z, Ż, Z̈])	[0,027;1,03;79,3]	[0,036;0,27;4,67]	[0,027;0,93;71]	[0,03;0,22;5,86]	[0,035;0,9;76]	[0,03;0,23;5,6]	[0,026;0,97;79,3]	[0,03;0,24;5,9]	[0,027;1;76]	[0,03;0,31;9,2]
RMS([Z, Ż, Z̈])	[0,011;0,29;16,4]	[0,01;0,082;1,5]	[0,012;0,28;15,3]	[0,0086;0,08;1,7]	[0,011;0,27;14]	[0,009;0,088;1,8]	[0,011;0,3;16,6]	[0,009;0,07;1,4]	[0,013;0,28;12,9]	[0,01;0,14;3,2]
$RMS(F_1^d)$	797	-	854	-	844	-	794	-	1306	-
	Passive b_2=2500Ns/m		**"Groudhook" control On-Off**		**"Groundhook" Vabs; K_g=0,65**		**"Groundhook" PID, K_g=0,65**		**MR "Groudhook" control On-Off"**	
$\int_0^{T_1} Z(t)dt$	0,35	0,24	0,35	0,25	0,34	0,28	0,33	0,27	0,36	0,36
Max([Z, Ż, Z̈])	[0,025;0,09;65]	[0,028;0,23;6,7]	[0,025;0,91;64]	[0,036;0,28;6,2]	[0,025;0,88;75]	[0,048;0,38;6]	[0,025;0,86;71,7]	[0,044;0,35;5,96]	[0,029;0,77;75]	[0,044;0,35;5,96]
RMS([Z, Ż, Z̈])	[0,012;0,26;13,5]	[0,009;0,095;2,1]	[0,011;0,26;14]	[0,01;0,096;1,9]	[0,011;0,27;14,2]	[0,012;0,07;1,96]	[0,011;0,28;15,6]	[0,0117;0,095;1,6]	[0,012;0,23;12]	[0,013;0,17;3,6]
$RMS(F_1^d)$	911,4	-	874	-	870	-	799	-	1367	-